Multiaxis and multibeam technology for high throughput maskless E-beam lithography

Hiroshi Yasuda,[a] Takeshi Haraguchi, Hidebumi Yabara, and Kouji Takahata
Development department, PARAM Corporation, Product Development Support Laboratory No. 2, Tama Techno Plaza, Tokyo Metropolitan Industrial Technology Research Institute, 3-6-1 Azuma-Cho, Akishima-Shi, Tokyo 196-0033, Japan

Hidekazu Murata, Eiji Rokuta, and Hiroshi Shimoyama
Faculty of Science and Technology, Meijo University, 1-501 Shiogamaguchi, Tempaku-Ku, Nagoya 468-8502, Japan

(Received 3 July 2012; accepted 29 October 2012; published 26 November 2012)

The authors have devised a new maskless E-beam lithography method which can achieve a throughput of 10 wph which the authors are calling a "multiaxis programmable shaped beam" (multiaxis PSB). It is a kind of massive parallel electron beam lithography wherein more than 250 000 beams write a wafer and the total beam current reaches a hundred microamperes. It may be difficult to write a pattern finer than 10 nm with more than 1 μA beam current at 50 kV with a single column because of blurring from Coulomb interaction, so the multiaxis PSB system divides all the beams into 87 groups where each group has 2500–10 000 beams formed by a small column arrayed in a 26 × 33 mm^2 lattice. The small column is called a column element (CE) and each CE has an emitter, apertures, deflectors, and small lenses. The key technologies of the multiaxis system are a lens, emitter, and blankers for individual beamlets. The authors have proposed new ideas for these issues and made fundamental experiments. © *2012 American Vacuum Society*. [http://dx.doi.org/10.1116/1.4767275]

I. INTRODUCTION

Through the past years many electron beam exposure systems have been proposed but those systems could not overcome the specific problems of very low throughput of the electron beam lithography system. The biggest reason was the beam blurring caused from Coulomb interaction wherein one could not have a large beam current and good resolution at the same time with a single beam.

The Mapper[1] solution is good for Coulomb interaction, because in this system the beam is divided into many beamlets with independent paths; however, to obtain a throughput of higher than 10 wph is difficult because there is only one electron emitter and the beamlets created by the electrostatic lens with a small convergence semi-angle seem to be weak. Also, to get a very fine emitter image the top of electron emitter must be very sharp, but this makes it difficult to ensure uniformity over the entire irradiated region. The DiVa[2] is also good for Coulomb interaction because in this system the beam is also divided into many beamlets with independent paths; however, in this method the demagnification ratio is around 1 and it may be difficult adequate accuracy of the beam. The MxM system[3] which Ion Diagnostic Inc has proposed also seems to mitigate the Coulomb effect; however, in this system only one electron emitter is responsible for the drawing of one dot and thereby the efficiency of the emitter is not maximized. We want to incorporate some sort of low-cost way to increase the number of the beamlets. The REBL Nanowriter,[4] which has been proposed by the KLA-Tencor Corporation, is a system using a digital pattern generator, such as a reflection mirror array. This system differs from the above three systems in that it suffers from the Coulomb effect. To eliminate this, it would be necessary to use a multicolumn, but and the electron emitter path must then be bent in order to configure the electron optical reflection system and to set up many columns like this would be difficult. We would like to propose a system that has the highest efficiency and one where accuracy and throughput can be realized simultaneously.

According to our simulation,[5] the blurring from the Coulomb interaction is proportional to $\mathrm{Vacc}^{-4/3}\cdot\mathrm{I}^{3/4}\cdot\alpha^{-1}\cdot\mathrm{L}^{3/4}$. Here, Vacc is the accelerating voltage, I is the total beam current, α is the beam convergence semi-angle on the object plane, and L is the total length of electron column (see Fig. 1).

For studies on the blurring due to the Coulomb interaction there are many other sources,[6–8] and the sometimes the value of the power of each factor is different. For example, the value of the power for Vacc varies as −4/3 or −3/2; for I as 3/4, 1, or 2/3; for α as −1, −5/4, or −4/3; and for L as 1, 3/4, or 2/3. We think these differences arise from differences between the various electron optical systematic assumptions. However, measures to overcome the Coulomb blur are not so difficult; we have to increase the factor which should be larger and decrease the factor which should be smaller and see if the degree of Coulomb blur can be reduced more efficiently. Because of our experiments we know that we cannot completely reduce the Coulomb effect using a single column, so we have to increase the number of columns. It seems that a higher accelerating voltage is better; however, with higher Vacc resist sensitivity becomes worse and is almost inversely proportional to the square of Vacc and so the current value must be increased to keep a high throughput. On the other hand, with higher Vacc the deflection efficiency will be lower and power consumption of various parts of

[a]Electronic mail: yasuda@param.co.jp

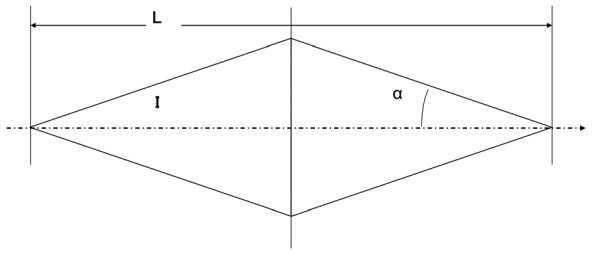

FIG. 1. Diagram explaining the blurring from the Coulomb interaction. The blurring is proportional to $Vacc^{-4/3}\cdot I^{3/4}\cdot\alpha^{-1}\cdot L^{3/4}$. Short column with large α, small Cs, and multiaxis column system are necessary.

system will be larger. Therefore, it is best not to increase Vacc to higher than 50 kV before any actual high throughput system is accomplished.

First, we propose a multicolumn system. Because we divide the total beam currents into 87 columns for a 300 mm wafer exposure, even in the case that we limit the maximum current to 1.28 μA by the exposure data, the total beam current can reach 111.36 μA, and such large currents will achieve high throughput. Figure 2 shows the 87 columns standing parallel wherein each column is called a column element (CE) and each CE covers a 26 × 33 mm field. This field size corresponds to one field of a photo stepper for mix and match use. Each CE has an emitter, round and square apertures, an illumination lens, a reduction lens, and an objective lens. We also use other techniques to maximize the current value further and in this article we describe some proposals to accomplish high throughput and high resolution at the same time.

II. CONCEPT OF PROGRAMMABLE SHAPED BEAM

Current mask costs are very high and, therefore, a maskless lithography system is strongly demanded. Figure 3 shows the principle of programmable shaped beam (PSB) wherein the electron beam from an emitter is split into several thousands of beams by a beam splitter and each blanker bends or lets the beam pass through individually. The lens gathers the beam on the hole of a round aperture and these

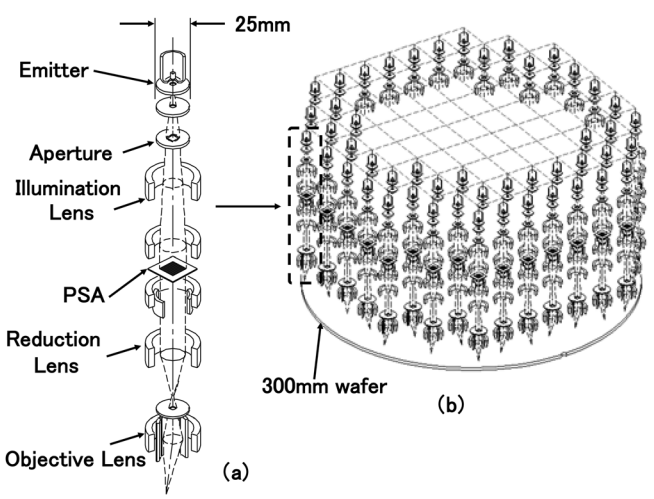

FIG. 2. Schematic of multiaxis PSB. (a) CE. (b) Schematic of 87 CEs on a 300 mm wafer.

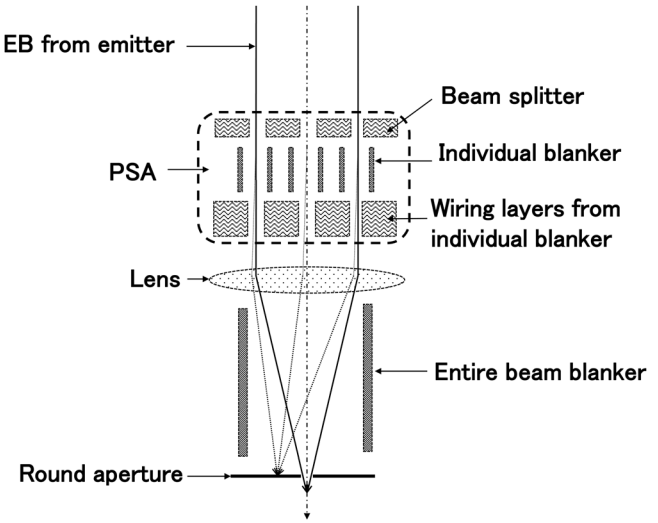

FIG. 3. Schematic explaining the principle of PSB.

beams are held on or off in static condition. After all of the individual blankers and beam deflectors are settled, the entire blanker is turned on and beam exposure is performed. Figure 4 shows the intended pattern to be exposed wherein each pixel of black square tiles is exposed and the grey square tiles are not exposed. Each black and grey square represents a pixel of size 16 nm in this case and the finest line width and gap are 16 nm.

Figure 5 shows the PSB exposure method where square beams are arrayed on the square lattice. The distance between adjacent beams is an integer multiple of the beam size and, therefore, a pattern which is represented by an integer multiple of the beam size is easily written. In Fig. 5, the beam size is 16 nm square on the objective plane and the distance between adjacent beams is 48 nm and, therefore, the repetition pitch of the beams is 64 nm. There are 2500 (50 × 50) beams in the 3.2 μm square field which are exposed at the same time and the exposure time is controlled by the opening time of the entire blanker. Some beams among the 2500 beams are in an off state as dictated by the bitmap data and others are in an on state and the 2500 beams are simultaneously deflected from the 1-1 site to the 1-16 site step by step, so the 3.2 μm square fields are exposed with a maximum of 16 shots. On the top surface of the PSA (programmable shaping aperture), 4 μm square holes are made with a 16 μm repetition distance. In this case, the reduction ratio is 1/250 from the PSA to the objective plane, so square area with an 800 μm side length has to be uniformly illuminated by an emitter. In Fig. 5, each hole has individual blanking electrodes but the distance between holes cannot be small

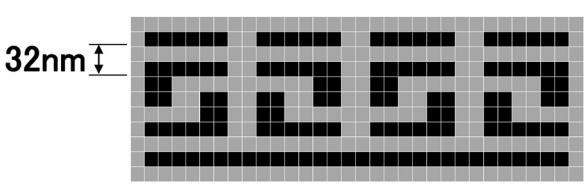

FIG. 4. Schematic explaining a PSB exposure method for drawing the micropixel square lattice.

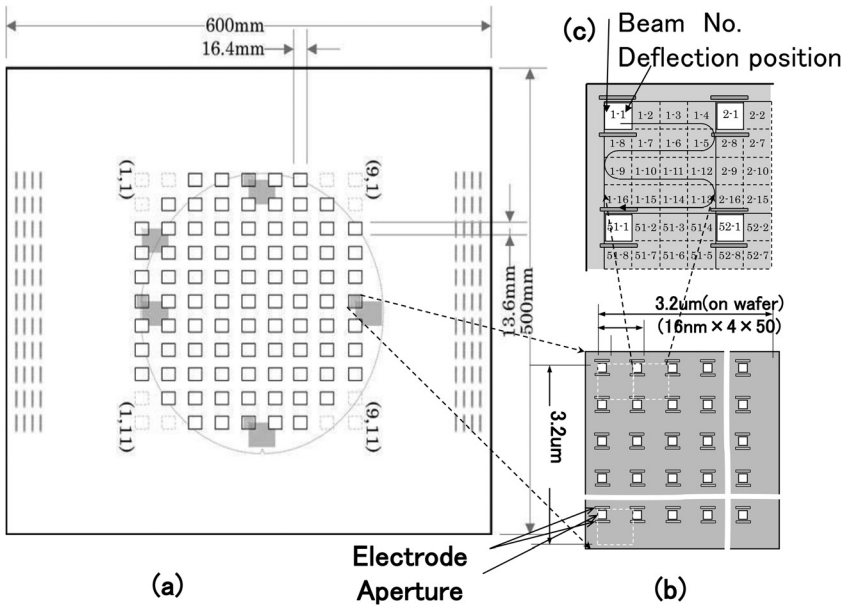

FIG. 5. Schematic explaining PSB exposure method and PSA unit. (a) PSA unit. (b) Programmable shaping aperture. (c) Schematic explaining an exposure method.

because the wires leading from the analogue amplifiers to the electrodes require a relatively large wiring area. PSA chips for the multicolumn are mounted on the same implementation board as the registers, analogue amplifiers, and the optical fiber cables for data transfer.

Table I shows the estimated throughput of the multiaxis PSB module which includes 87 CEs and uses a 16 nm hole and space pattern, a resist sensitivity of 120 μC/cm^2, and a current density of 400 A/cm^2. In this case, an average of 1920 electrons are incident into the hole pattern of 16 nm square. The number of electrons varies according to the Poisson distribution, so the standard deviation of the number of electrons, σ, is 43, which is the square root of 1920, and if we take a variation of 3σ the electron number variation is 6.8%. Shot noise is decreased with a decrease in the resist sensitivity, but throughput becomes lower and, therefore, resist sensitivity can be optimized for the dimensions of the hole.

TABLE I. Estimation of the throughput of the PSB for exposure of a 16 nm 1:1 hole layer.

Resist sensitivity	120 μC/cm^2
Current density	400 A/cm^2
PSA blanker settling time	50 ns
Settling time for minor deflector	85 ns
Minor deflector jumping step inside 64 nm square field	32 nm
Settling time for major deflector	200 ns
Major deflector scan width	50 μm
Maximum current	1.28 μA
Number of shots in 3.2 μm region	8
Time of shots in 3.2 μm region	3.055 μs
Time for 3.2 × 48 μm^2 band	45.825 μs
Pure writing time for 26 × 33 mm^2	267 s
Number of stripes of 48 μm width	542
Stage velocity in Y direction (33 mm)	67 mm/s
Stage acceleration in Y direction to wrap	2.0 m/s^2
Time required to wrap from stripe to stripe	0.067 s
Total time required to wrap	36.32 s
Traveling time for 50 μm in X direction	0.014 s
Other overhead time	50 s
Total time	353 s
Throughput	10.2 wph

The total current through the 2500 holes (16 nm square and 400 A/cm^2) is 2.56 μA, which is too large for the 16 nm hole because of blurring from the Coulomb interaction, and so we control the bitmap data so as not to exceed a maximum current of 1.28 μA in the PSB. In this case, we turn off the electrons through half of the holes and turn on the electrons through half of the holes. If we turn on electrons through all the holes we can expose the resist with four shots, but we divided the total exposure into eight shots to expose the pattern.

The major deflector scan field is $\pm$25 μm and the stripe width is 50 μm and 15 shots of 3.2 μm square can be exposed. The settling time for the PSA blanker is 50 ns, for the minor deflector is 85 ns, for the major deflector is 200 ns, creating a total exposure time for a region of 3.2 μm by 48 μm of 45.825 μs. Therefore, we can expose the pattern with a velocity of 67 mm/s on the fly in the Y-direction which has a 33 mm length. There are 542 stripes each with 48 μm width in the X-direction, which has a total of 26 mm in length.

The stage acceleration in the Y-direction to wrap is 0.2 G, which is 2.0 m/s^2, so the time required to wrap a stripe is 67 ms creating a total time required to wrap of 36.32 s. In the case of wrap, the stage moves 50 μm per step in the X-direction, and with an acceleration of 0.1 G the time required is within 0.014 s, which is included in the wrap time in the Y-direction. If we require 50 s for wafer handling and optical alignment, the total time per wafer is 353 s and the throughput is 10.2 wph.

III. KEY TECHNOLOGIES FOR MULTIAXIS PSB

A. Lens with a permanent magnet

The blurring from the Coulomb interaction is proportional to $Vacc^{-4/3}\cdot I^{3/4}\cdot\alpha^{-1}\cdot L^{3/4}$; therefore, to make the column short is very important. Moreover using a large convergence semi-angle of the objective lens (α) is very effective, and we found that from 10 to 15 mrad is better to decrease the Coulomb interaction as shown in Fig. 6. However, in the 15 mrad case the spherical aberration will be large and, therefore, a small spherical aberration coefficient with a value around 6 mm is necessary because the spherical aberration is proportional to the cube of the convergence semi-angle. In addition, the radius of the circle of least confusion ($=1/2Cs\cdot\alpha^3$) is found to be 10 nm. Even in this case, the Coulomb interaction adds a blurring of 5 nm with a current more than 1 μA.

Therefore if we use a large current, it is important to have a refocusing technology in which the focusing parameter such as magnetic field strength or beam voltage in the path is changed according to total beam current value. Such a technology will require strict conditions to the system and, in addition, after the entire beam current changes it takes a certain amount of time for refocusing signal settling; therefore, in a state of a continuously scanning beam, as in the usual massive parallel method, it is difficult to use this refocusing technique. After the entire beam current has settled and the refocusing signal has settled, the entire beam blanker is released, as shown in Fig. 4, for an exposure shot. In this way, the PSB system and a step-by-step deflection and exposure are performed.

Figure 7 shows the lens for the multiaxis. The required conditions for the lens are as follows: the size must be smaller than 25 mm with a magnetic field larger than 0.4 tesla and a power consumption smaller than 4 mW. These conditions are chosen to minimize heat generation even when a large number of column cells are used. For this reason, a permanent magnet is suitable for the magnetic lens

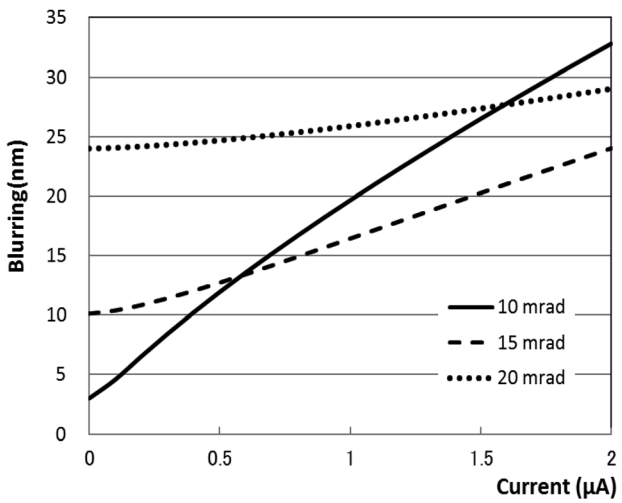

FIG. 6. Blurring from an axial spherical aberration and the Coulomb interaction. The horizontal axis represents the beam current value and the vertical axis represents the beam blurring (nm). Cs (spherical aberration coefficient) is 6 mm.

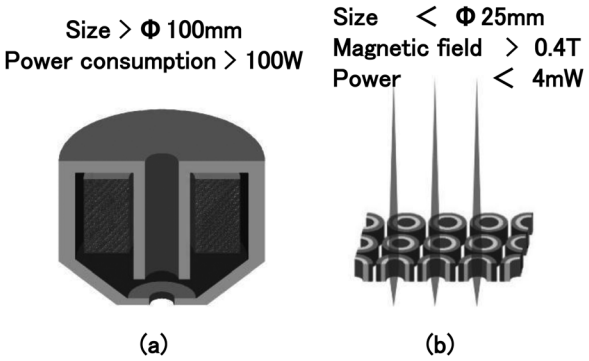

FIG. 7. Schematic diagrams of traditional magnetic lens (a) and permanent magnet lenses (b).

where the permanent magnet is managed so that the temperature stability is adequate and is manufactured with high accuracy with the error compensated for at approximately $\pm 2\%$ with a small coil.

Figure 8 shows a fundamental evaluation of the permanent magnet lens using a scanning electron microscope. Two SEM images of the 0.6 μm square pattern which is made of heavy metal on a silicon chip are compared with and without the permanent magnet lens. There is no apparent difference between the two images, and so we conclude that the lens of the permanent magnet in principle has no severe problem.

B. Emitter with a rhenium sheath

In the emitter, illumination uniformity, high brightness, and a long life time are required. Figure 9 shows the low temperature, thermal field emitter (TFE) with a strong electric field which is concentrated at the top flat surface of the 80 μm square LaB_6 pile. In the round hole at the top surface of a sharpened rhenium tip, an LaB_6 pile, of length 500 μm, is set with a protruding 20 μm tip. The protruding of the LaB_6 is essential, because when the LaB_6 and rhenium tips start at the same height, sublimation reduces the height of the surface of only LaB_6.

The goal of the emitter is to have a current emission of 100–200 μA, a brightness of 6×10^5 A/cm^2, and irradiation uniformity of more than 95% at a temperature of 1700 K. Figure 10 shows a photograph of the actual LaB_6 TFE tip with a rhenium sheath. Figure 11 shows the emission pattern of the emitter on the fluorescent screen with experimental conditions of an LaB_6 temperature of 950 K, an extraction voltage of 6 kV, and an emission current of 10 μA. In this experiment, however, the temperature is too low and it is necessary to improve the condition. Despite the low temperature, the square area is brightly illuminated and radiation from the surrounding surface sharply decreases showing that the sidewall protection of the LaB_6 tip is effective which contributes to lower power consumption.

C. PSA device

Figure 12 shows the PSA device in which we use new technologies. We had a lot of experiences working with

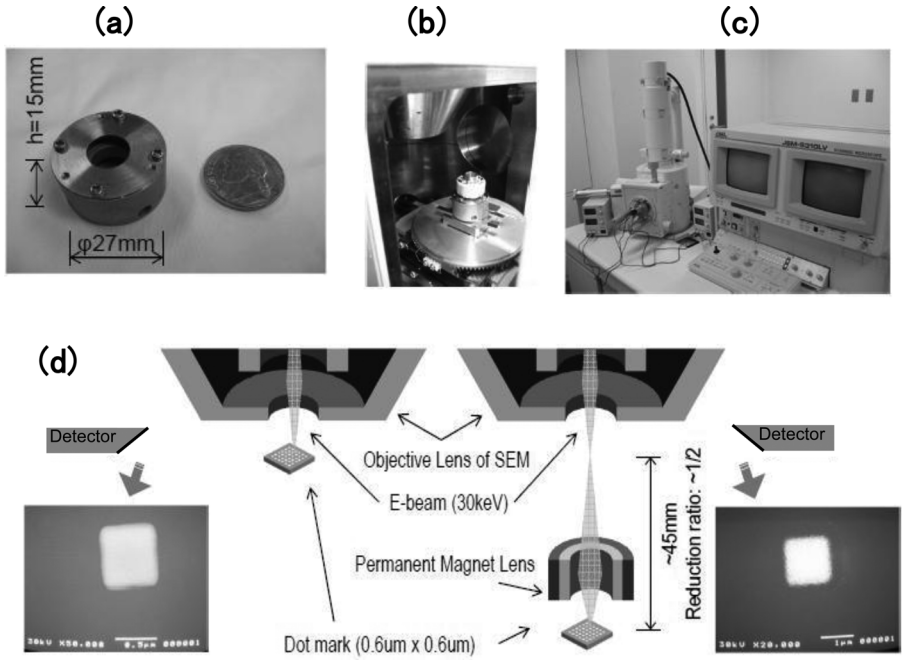

FIG. 8. Fundamental evaluation of the permanent magnet lens using SEM. (a) Test piece of permanent magnet lens. (b) Permanent magnet lens setting in specimen chamber of SEM. (c) Overview of SEM (JEOL: JSM-5310LV). (d) Comparison of with and without permanent magnet lens.

blanker aperture arrays,[9] and conventional blankers had two major problems. The first is that the insulator film is easily broken down by 50 kV electron irradiation for more than a few days. This phenomenon also applies to electrons which are accelerated at other voltages, for example, at 5 or 10 kV. It is also well known that the lifetime for the number of write operations of the high frequency silicon oxide film flash memory from several volts to several tens of volts is just a few days in constant currents. Thus, a silicon oxide film has not the necessary resistance to act as insulation for the required long-term electron currents.

The second problem we experienced is that high aspect ratio electrodes were difficult to make by electro-plating using conventional methods. New electrodes are created by forming an impurity diffusion layer on the sidewall of the semiconductor substrate. The PSA is made of Si and a PN junction for the insulating material instead of a silicon oxide film and silicon nitride film whereas the electrode is made of Ntype-doped Si and a +5 volt is supplied to bend the electron beam. The above configuration means that a PN junction diode with a reverse bias applied is used as an electrode with the opposing electrodes grounded to the ground potential. The aspect ratio of the electrodes is made high with bonded wafers. Insulation for the wiring pattern from the individual blanker electrodes of the PSA device is performed by applying a reverse bias to the PN junction. The reason for the proposed method of production of the PSA device is based on the following facts: silicon and other semiconductors and PN junctions or PIN junctions have a long lifetime under electron irradiation as guaranteed by several tens of years of experiments.

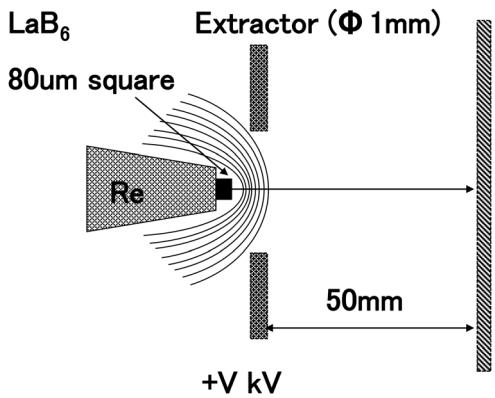

FIG. 9. Schematic explaining a low temperature thermal field emitter of LaB6 with a sharpened rhenium sheath.

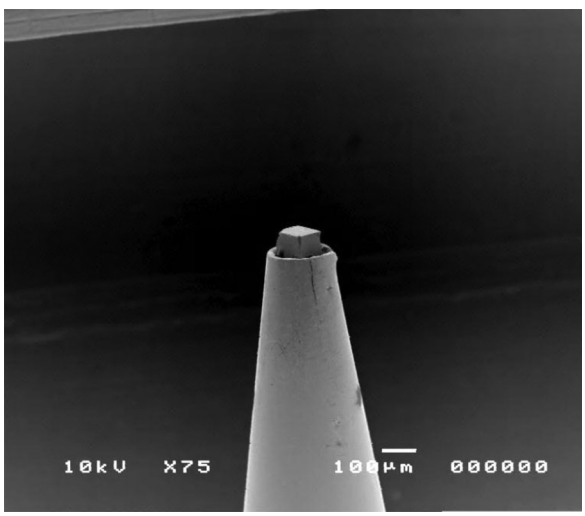

FIG. 10. SEM image of flat top LaB_6 cathode embedded into rhenium sheath.

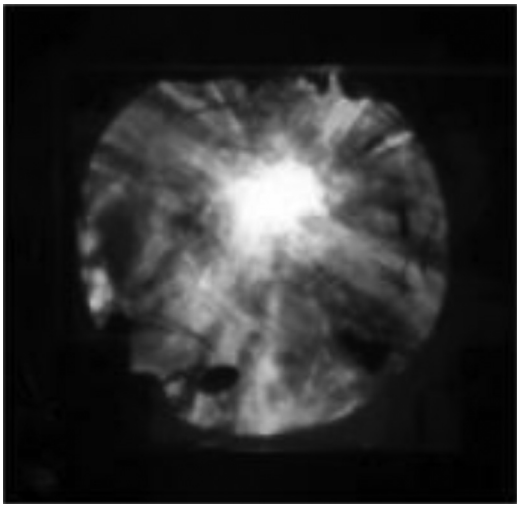

FIG. 11. Typical example of emission pattern of LaB_6 cathode embedded into rhenium sheath in TFE mode.

IV. ROADMAP

Figure 13 shows a roadmap of the performance of the multiaxis PSB. We believe the roadmap accordingly for 16, 11, and 8 nm half pitch (HP) would be required for the year 2014, 2016, and 2018, respectively. The data transfer rate and the number of beams can be varied to fit the pattern generation as, for example, from 16 nm using 2500 beams to 8 nm using 10 000 beams. To provide 2500 bitmap data for each 10 MHz shot cycle requests 25 Gbps per CE. Including other data, for example, beam position, the data request data transmission rate of 47.75 Gbps per CE is required. Total data transfer rates, therefore, may be around 5 Tbps in a system using 87 columns. These high speed data transfer rates can be achieved by a serial-to-parallel conversion large scale integration, using 200–500 optical fibers and external circuits for data transfer. It will be required to have an equivalent reduction rate of the hole size of the PSA corresponding to the pattern generation, though this may make the production of the PSA difficult. The reduction rate of the column can also be changed.

In Table II, the exposure dose and current density are not changed corresponding to the pattern generation, though the reduction ratio is 1/250. It will also be necessary to change some parameters along with the pattern rules. While keeping a constant throughput, such as current density, the number of columns or the shot time should be changed. It will be necessary to devise a constant shot noise in a hole for a different generation, but we would like to focus on realizing the targets of 16 nm generation at this time. The measures necessary to create the necessary number of electrons in the hole for each desired generation are a challenge for the future.

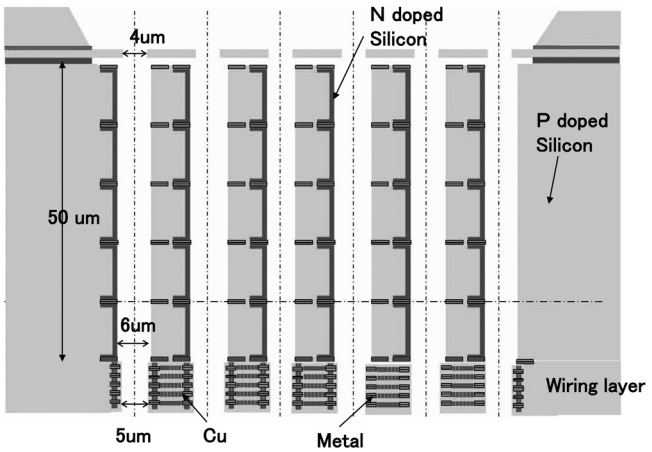

FIG. 12. Schematic explaining a structure of high aspect ratio PSA.

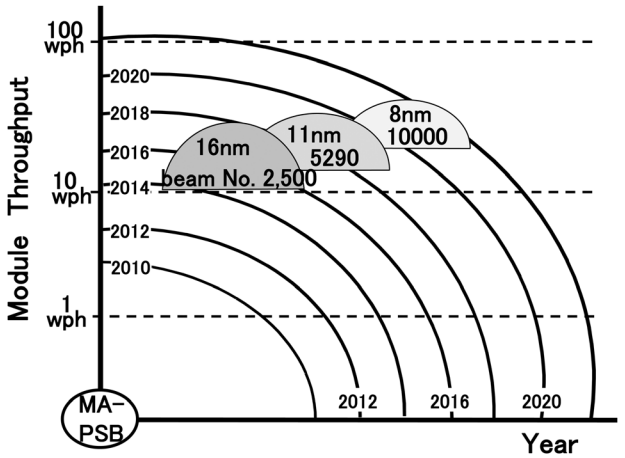

FIG. 13. Schematic explaining a road map of multiaxis PSB.

V. DISCUSSIONS

We know that the PSB is different from other massive parallel systems in the drawing strategy, for in this method only a pattern whose size is an integer multiple of the beam size can be drawn with the minimum number of shots. However, we want to know whether a lithography tool should not have such a restriction. We can get a high throughput instead of this restriction. Also, is halftone exposure necessary for some limited process layers?

It is sometimes pointed out that our system seems much closer to the massive parallel system of the Multibeam

TABLE II. Relationship of PSA, hole size, pattern generation, and data transmission speed.

	16 nm HP	11 nm HP	8 nm HP
Year	2014	2016	2018
Beam size (nm)	16	11	8
Number of CEs		87	
Number of beams	217 500 ($50 \times 50 \times 87$)	451 008 ($72 \times 72 \times 87$)	870 000 ($100 \times 100 \times 87$)
Hole size (μm)	4.0	2.75	2.0
Data transmission speed (Gbps/CE)	47.75	99.01	191
Current density (A/cm^2)		400	
Current/beam (nA)	1.024	0.484	0.256
Max. total current (μA)		111.36 ($1.28\ \mu A \times 87$)	
Throughput (wph)		10	

Corporation as proposed by Dr. David K. Lam. Our system also has a multicolumn at the same distances as the fields of the photo stepper. However, in the system of the Multibeam Corporation the number of internal beams may be a single fixed shaped beam, while our system uses several thousands of beams with a two-dimensional square lattice array inside a column. Our multicolumn also has two-dimensional square lattice array columns. This system aims not only at complementary lithography but also at the application of other maskless processes such as layers of hole of memories of one to one hole and space, logic holes or conventional wiring.

VI. CONCLUSIONS

We have proposed a multiaxis PSB tool with a large current and a 10 wph electron beam tool. The large current will be created by a short column; a large convergence semiangle, α; a small spherical aberration and refocusing for each exposure shot. A PSB is suitable for minimizing the pattern data and a fixed shot with a multibeam is good for simplicity and for refocusing with reduced Coulomb interaction.

We proposed and performed a basic evaluation of a new emitter and permanent magnet lens. There are restrictions on this tool that make it suitable only for the wiring and hole layer, though a high throughput is not a restriction. Also, we proposed a new PSA electrode and wiring system.

ACKNOWLEDGMENTS

The authors would like to thank Masanori Kubota and Tomohira Tabata at the Institute of Engineering Innovation, Graduate School of Engineering, the University of Tokyo for making the LaB_6 emitter. The authors also would like to thank Kunihiro Asada at the VLSI design and education center of University of Tokyo for useful discussions.

[1]E. Slot *et al.*, Proc. SPIE **6921**, 69211P (2008).
[2]T. R. Groves, D. Pickard, B. Rafferty, N. Crosland, D. Adam, and G. Schubert, Microelectron. Eng. **61**, 285 (2002).
[3]N. W. Parker, A. D. Brodie, and J. H. McCoy, Proc. SPIE **3997**, 713 (2000).
[4]P. Petric *et al.*, Proc. SPIE **7271**, 727107 (2009).
[5]H. Shimoyama, "Computer simulation of energetic and spatial Boersch effect in electron optical instruments," private communication (unpublished work).
[6]T. Groves, D. L. Hammond, and H. Kuo, J. Vac. Sci. Technol. **16**, 1680 (1979).
[7]G. H. Jansen, Nucl. Instrum. Methods Phys. Res. A **298**, 496 (1990).
[8]J. L. Mauer, H. C. Pfeiffer, and W. Stickel, IBM J. Res. Dev. **21**, 514 (1977).
[9]H. Yasuda, S. Arai, J. Kai, Y. Ooae, T. Abe, Y. Takahashi, S. Fueki, S. Maruyama, and T. Betsui, Jpn. J. Appl. Phys., Part 1 **32**, 6012 (1993).